ACS OMEGA

http://pubs.acs.org/journal/acsodf

Article

Pressure-Induced Transition from Spin to Superconducting States in Novel MnN_2

Li Li, Xingbin Zhao, Kuo Bao,* Defang Duan, and Tian Cui*

Cite This: *ACS Omega* 2021, 6, 21830−21836

Read Online

ACCESS | Metrics & More | Article Recommendations | Supporting Information

ABSTRACT: The connection between magnetism and superconductivity has long been discussed since the discovery of Fe-based superconductors. Here, we report the discovery of a pressure-induced transition from a spin to a superconducting state in novel MnN_2 based on ab initio calculations. The superconducting state can be obtained in two ways: the first is the pressure-induced transition from an AFM-$P2_1/m$ to an NM-$I4/mmm$ phase at 30 GPa, while the other is the pressure-induced transition from an FM-$I4/mmm$ phase to magnetic vanishing at 14 GPa, which leads to a structural transition with the distortion of octahedrons to tetragonal pyramids. NM-$I4/mmm$-MnN_2 is superconductive with $T_c \approx 17.6$ K at 0 GPa. In the second way, electronic structure calculations indicate that the system transforms from a high-spin state to a low-spin state due to increasing crystal-field splitting, causing disappearance of magnetism; more electron occupancy around the Fermi level drives the emergence of superconductivity. Remarkably, $I4/mmm$-MnN_2 can achieve mutual spin-to-superconducting state transformation by pressure. Moreover, the AFM-$P2_1/m$-MnN_2 phase is extremely incompressible with the hardness above 20 GPa. Our results provide a reasonable and systematic interpretation for the connection between magnetism and superconductivity and give clues for achieving spin-to-superconducting switching materials with certain crystal features.

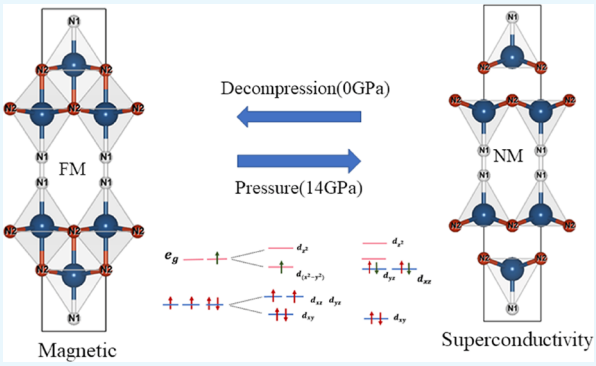

INTRODUCTION

Transition from spin to superconducting states has been one of the central themes of condensed-matter physics, which is often accompanied by a change in the spin state of the electron. This transition only exists in unconventional superconductors, like Fe-, Mn-, and Cr-based, and heavy fermions.[1−5] However, the mechanism of superconductivity has long been discussed. Recently, antiferromagnetic fluctuation has been a common interpretation for the formation of Cooper pairs for Fe-based systems, thus inducing the emergence of superconducting states.[6] The magnetic matrix seems to have a positive effect on the formation of superconductors. However, for a weak-coupling superconductor by electron−phonon interactions based on Bardeen−Cooper−Schrieffer theory, magnetism and superconductivity do not coexist, and magnetism often hinders its superconductivity. The ground state of the material should be a nonmagnetic state, like hydrogen-rich compounds with a high superconducting transition temperature (T_c).[7−9] This greatly limits the search for new superconducting materials and hinders the exploration of the mechanism of spin to superconducting transition.

Compounds of transition-metal (TM) nitrides have been drawing considerable attention owing to their outstanding mechanical, superconducting, and magnetic properties.[10−16] However, the synthesis of "pure" TM nitride compounds or compounds with an integral ratio by conventional high-temperature methods is difficult because of the unstable thermodynamics of nitrides at high temperatures. The application of high pressure (HP) is an effective and clean method to adjust the distance between atoms, to change the mode of electron occupation and spin state, and thus to synthesize new materials with novel properties,[17,18] such as the metal to insulator transition with the Mott transition under HP in MnO. The electrons from the high-spin state to the low-spin state transition drive the collapse of magnetic moment, due to an increase in the crystal-field splitting.[19] Ferromagnetic bcc iron was reported to transform to an hcp nonmagnetic (NM) state at 15 GPa with T_c below 2 K.[20] For the first unconventional Mn- and Cr-based superconductors,

MnP and CrAs,[3,4] the T_c values are about 1 and 2 K under HP, respectively. Because a Mn atom has five electrons in the 3d orbital, which has the largest number of unpaired electrons in the periodic table, Mn nitrides have rich stoichiometric magnetic phases, such as ε-Mn_4N with ferrimagnetic (FiM)

Received: July 7, 2021
Accepted: August 9, 2021
Published: August 16, 2021

https://doi.org/10.1021/acsomega.1c03583
ACS Omega 2021, 6, 21830−21836

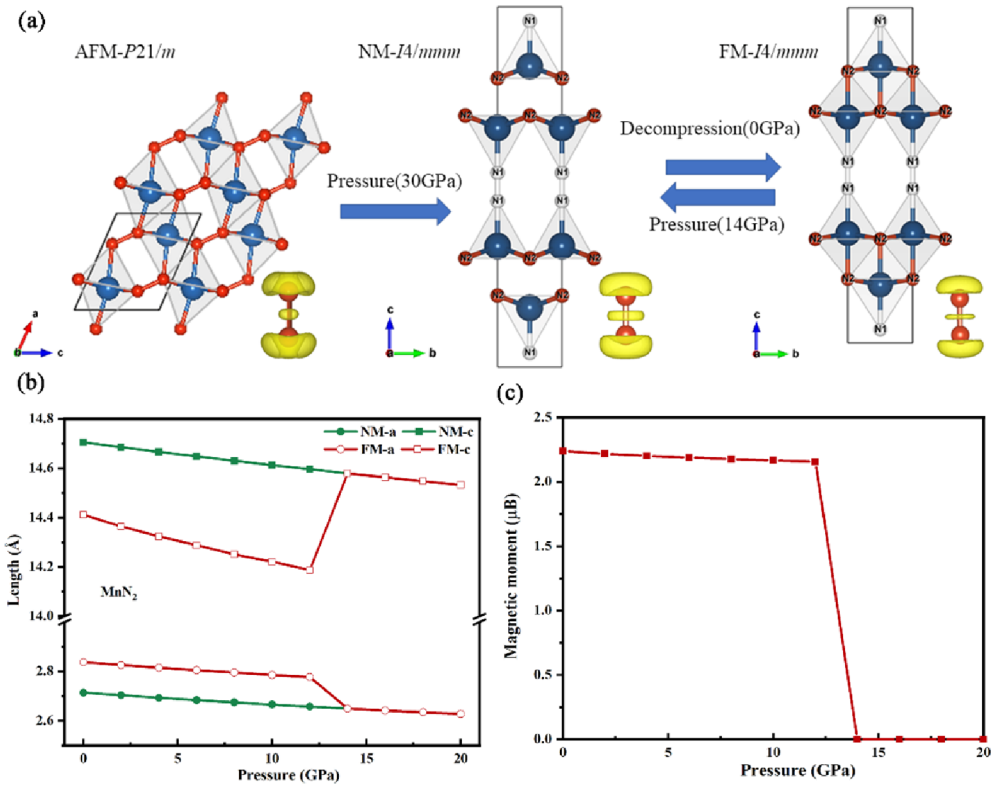

Figure 1. (a) Crystal structure and process of phase transition: the electronic localization function (ELF) at 0 GPa of AFM-$P2_1/m$-MnN_2 and FM-$I4/mmm$ with an isosurface value of 0.6 and NM-$I4/mmm$ with an isosurface value of 0.75 at 14 GPa. Blue, white, and red spheres denote Mn, N1, and N2 atoms, respectively; (b) lattice parameters vary with pressure; and (c) magnetic moment varies with the pressure of FM-$I4/mmm$.

order[21] and ζ-Mn_2N_1, θ-MnN, and η-Mn_3N_2 phases with antiferromagnetic (AFM) order, which are all confirmed by neutron diffraction experiments.[22−24] Generally, magnetic order disappears or is suppressed under HP; thus, it might be interesting to know whether superconductivity originates when the magnetic order vanishes under HP.

In this study, we search Mn−N compounds from 0 to 40 GPa with the USPEX code. The N-rich new structures $P2_1/m$-MnN_2 and $I4/mmm$-MnN_2 have been predicted, and they all can remain at ambient pressure. A pressure-induced transition from the spin to superconducting state due to structural phase transition has been found in the novel MnN_2, and we explain the reason for the disappearance of magnetism and emergence of superconductivity according to crystal field theory. The T_c of NM $I4/mmm$-MnN_2 decreases with increasing pressure and can reach 17.6 K at 0 GPa. Remarkably, $I4/mmm$-MnN_2 can achieve spin-to-superconducting state mutual transformation by pressure. Moreover, the AFM-$P2_1/m$-MnN_2 phase is extremely incompressible with the hardness value above 20 GPa.[2,3]

RESULTS AND DISCUSSION

We search magnetic structures at high pressure and find thermodynamically, kinetically, and mechanically stable N-rich MnN_2. The AFM-$P2_1/m$-MnN_2 phase is predicted to exist between 7 and 30 GPa, and the NM-$I4/mmm$-MnN_2 becomes stable above 30 GPa (Figure S1). The phonon spectrum of these structures is shown in Figure S2. The lattice constants of the AFM-$P2_1/m$-MnN_2 phase are a = 4.822 Å, b = 2.832 Å, and c = 3.921 Å at 0 GPa (Table S1). The Mn atoms are coordinated to six N atoms, forming a distorted octahedron. The edge-sharing octahedron layers are connected by the N−N bonds. In FeN_2, this structure was proposed to be in the NM state.[25] The closest N−N distance is 1.308 Å, and it is comparable to that in FeN_2 (1.326 Å), both of which are within the range of single and double bonds. Above 30 GPa, the AFM-$P2_1/m$ phase transforms into the NM-$I4/mmm$ phase. The Mn atom is located in a pyramid made up of one N1 atom and four N2 atoms, as shown in Figure 1a. It is worth noting that the energy of the FM (ferromagnetic) $I4/mmm$ phase is lower than that of the NM-$I4/mmm$ phase at 0 GPa (Figure S3), and the results of decompression are the same as those in Figure 1c,d. Thus, pressure-induced mutual transformation of the FM state to an NM state in $I4/mmm$ is achieved. To the best of our knowledge, no FM MnN compounds have been reported so far. The FM state (a = 2.837 Å and c = 14.411 Å) is composed of a stacked layer of distorted octahedrons connected by nitrogen−nitrogen bonds. Our calculations manifest that when the FM-$I4/mmm$ phase is subjected to pressure, the magnetic moment completely disappears at 14 GPa. It undergoes abnormal negative axial compression; precisely, it expands along the c axis in the NM state (a = 2.649 Å and c = 14.579 Å at 14 GPa), which might be connected with the vanishing of the magnetism. This phenomenon is also observed in compressed CrAs,[3] and there is a sudden increase in lattice constant b by ∼4%, with a suppression of antiferromagnetism. This phase transition is also supported by the lattice parameters (Figure 1b,c), and the lattice parameters of NM and FM states are exactly the same after 14 GPa, which pressure could be easily achieved experimentally nowadays.[7,13] All of these phases can be preserved at 0 GPa, and the phonon spectra are shown in

https://doi.org/10.1021/acsomega.1c03583
ACS Omega 2021, 6, 21830−21836

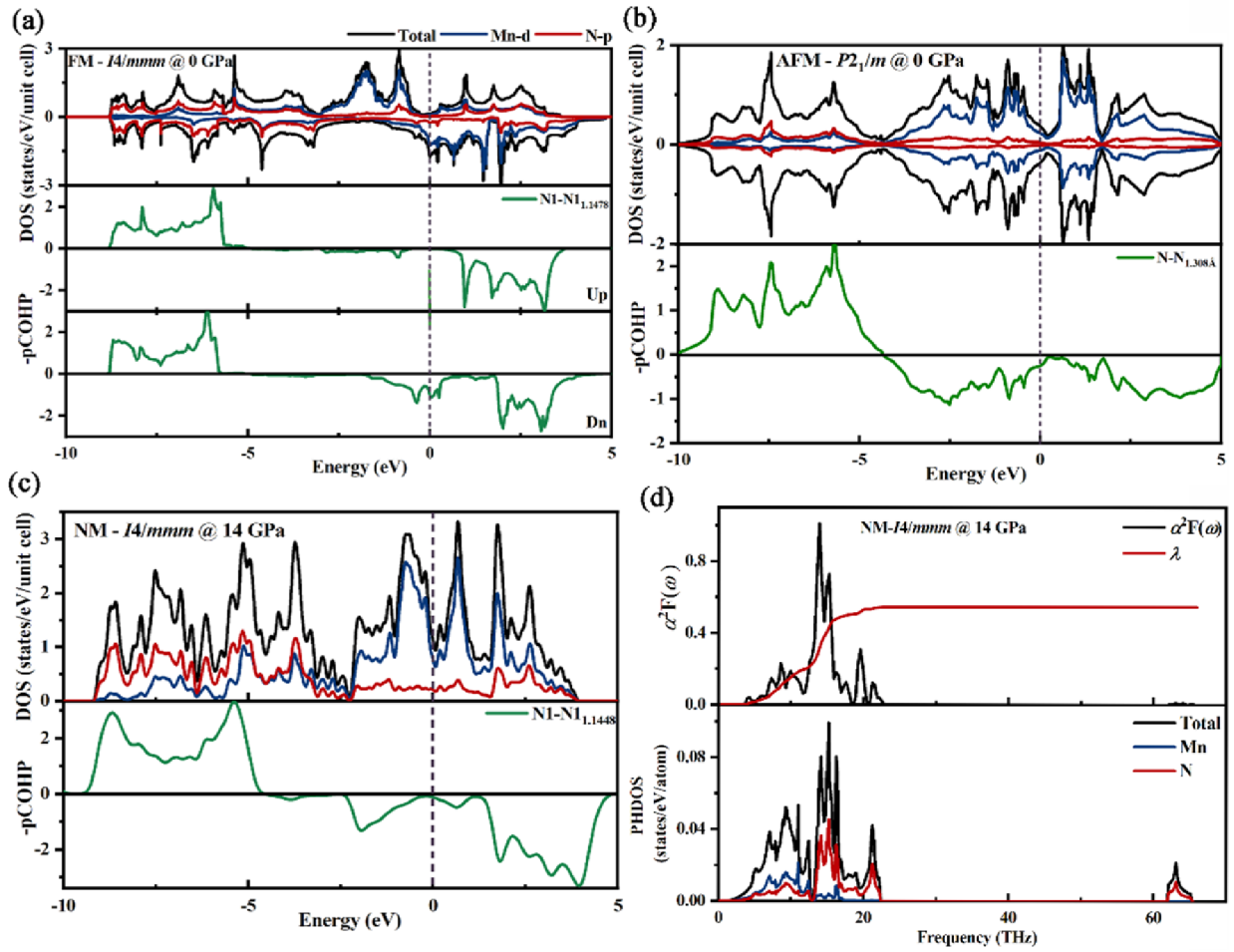

Figure 2. Projected electronic DOS and the COHP of MnN_2: (a) FM-*I*4/*mmm* state at 0 GPa, (b) AFM-$P2_1/m$ state at 0 GPa, (c) NM-*I*4/*mmm* state at 14 GPa, and (d) Eliashberg spectral function $\alpha^2F(\omega)$ together with the electron−phonon integral λ (top) and PHDOS (bottom) of NM-*I*4/*mmm* at 14 GPa.

Figure S2. Thus, there are two routes to obtain the NM state (Figure 1a).

In the FM state, the bond lengths of Mn−N1 and Mn−N2 along the *c* axis are 1.926 and 1.959 Å, respectively. Due to the elongation of the *c* axis in the NM state, the distance between Mn and N2 planes increases to 1.999 Å, which results in the formation of the pyramid layers. To compensate, the Mn−N1 bond within a pyramid becomes shorter, which strengthens the interaction between Mn and N1. The N1−N1 bond length in the NM state is 1.145 Å, which is similar to that (1.147 Å) in the FM state, is shorter than the typical N═N bond length, 1.210 Å, and is close to that of molecular N_2 (1.100 Å). Pressure drives six-coordinated Mn atom-stacked octahedra (MnN_6) in the FM-*I*4/*mmm* MnN_2 into five-coordinated, edge-sharing tetragonal (MnN_5) pyramids instead of distorted octahedrons as in the AFM-$P2_1/m$ state. The ELF also demonstrated the existence of covalent interactions between N−N bonds (Figure 1a). Moreover, isostructural *I*4/*mmm*-FeN_2 and CrN_2 have been considered; however, the phonon spectra have shown imaginary frequency in them except for FM FeN_2. For FM FeN_2, thermodynamics is unstable at 200 GPa and all of these show FM order and cannot be press to the NM state. The tendency of lattice parameters of CrN_2 and FeN_2 in their unstable range is discrepant compared with MnN_2, and there is no axial negative compression (see Figure S4).

To further understand the electronic properties of MnN_2, the partial electronic density of states (PDOS) are calculated (Figure 2). The three phases are all metallic, and the Mn 3d orbital contributes to the electronic DOS at the Fermi level significantly. For the AFM-$P2_1/m$-MnN_2 phase, the DOS of the spin-up and spin-down are almost equal, with the AFM state imparting 1.631 μ_B per Mn atom. In the FM-*I*4/*mmm* state, the spin-up state exhibits poor metallicity. Owing to the highly unequal electron occupation in both the spin channels of the Mn and N atoms, as shown in Figure 2a, both Mn and N atoms contribute to the magnetic moment. In each Mn 3d orbital, the spin-up and spin-down states contribute charges of ∼3.62 e^- and 1.43 e^-, respectively, resulting in a net moment of 2.19 μ_B. The N 2p orbital also imparts a small moment, with moments of 0.08 and 0.02 μ_B for N1 and N2, respectively. The NM phase acts as a good metallic material with highly dispersive bands that cross the Fermi level; Mn 3d and N 2p electrons exhibit the same peak at the same energy of the Fermi level, representing a strong interaction between the N 2p and Mn 3d states.

Since the discovery of the first Mn-based superconductors by Cheng et al.,[4] T_c values of the isostructural B31-type Mn*X* (*X* = N, P, As, Sb) compounds have been calculated by first-principles and are in good agreement with the experimental results (0.5−4 K) and the suitable DOS at the Fermi level in the NM-*I*4/*mmm* phase.[26] Thus, we examined the super-

https://doi.org/10.1021/acsomega.1c03583
ACS Omega 2021, 6, 21830−21836

conductivity in the NM $I4/mmm$-MnN_2 phase at 14 GPa. The partial phonon density of states (PHDOS) and the Eliashberg spectral function $\alpha^2F(\omega)$, together with the electron−phonon integral (λ) of NM-$I4/mmm$, are shown in Figure 2d. The electron−phonon coupling (EPC) was calculated based on the Allen−Dynes-modified McMillan equation,[27] with $\lambda \approx 0.57$ and $T_c \approx 9.6$ K. In PHDOS, the low-frequency ranges (below 17 THz) were dominated by Mn and N atoms, while the small-scale high-frequency ranges (61−64 THz) were mainly related to N atoms.

To understand the connection between the emergence of superconductivity and the vanishing of magnetism, we study the projected electronic DOS of the Mn 3d orbital of $I4/mmm$-MnN_2 in both the FM and NM states (Figure 3) and

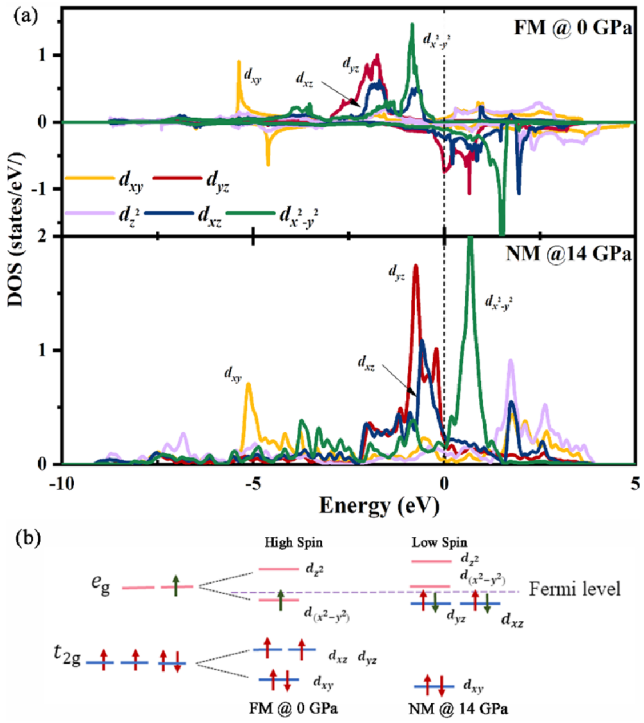

Figure 3. (a) Mn 3d orbital's projected DOS of FM and NM-$I4/mmm$ MnN_2. (b) Sketch of electron occupation. Notice that electrons are not integers.

electronic band structures (Figure 4). The Mn 3d orbital splits into two modes: threefold degenerate t_{2g} orbitals (d_{xz}, d_{yz}, and d_{xy}) and doublet degenerate e_g orbitals ($d_{x^2-y^2}$ and d_{z^2}). The spin-up electrons of the FM phase are mostly in the $d_{x^2-y^2}$, d_{xz}, d_{yz}, and d_{xy} orbitals. As for spin-down, the electrons occupy the d_{xy} and d_{yz} orbitals. The spin-up electrons outnumber the spin-down ones. As mentioned above, MnN_2 under pressure shrinks along the a and b axes and elongates along the c axis, and the distances between four N2 atoms at the bottom of a pyramid decrease. Because the $d_{x^2-y^2}$ orbital collides head-on with four N2 atoms, the orbitals pointing to N2 atoms within a (MnN_5) pyramid strongly repel each other due to the increasing crystal-field splitting, which pushes the $d_{x^2-y^2}$ orbital above the Fermi level. Subsequently, the electrons that were in the $d_{x^2-y^2}$ orbital would occupy the lower-energy d_{xz} and d_{yz} orbitals, and the system transforms from a high-spin state to a low-spin state, which causes the electrons in the d_{xz} and d_{yz} orbitals to be paired up. As a result, on the one hand, the magnetism disappears; on the other hand, it is extremely conducive to the formation of Cooper pairs because more electrons are occupied in the d_{xz} and d_{yz} orbitals close to the Fermi level. Meanwhile, the accumulation of electrons near the bottom of pyramids also results in the repulsion between pyramid layers, which leads to the elongation of the c axis.

The band structure also gives clues of the appearance of superconductivity. The bands in the NM state tend to be parallel and are close to the Fermi level, which means a dense electron occupation. The crystal orbital Hamilton population (COHP) shows electrons in the partially filled π antibonding states and the improved metallicity. The ELF (Figure S5) of the NM state shows that more electrons are localized between atoms than the FM state and improved electrical conductivity, which played an important role in the emergence of superconductivity. To understand the change in T_c under pressure, we also examine T_c in this phase at 0, 20, and 40 GPa, respectively, and find that it decreases with increasing pressure ($T_c \approx 17.6$, 9.6, 4.6, and 3.1 at 0, 14, 20, and 40 GPa, respectively). Intuitively, this is the reason for the gradually smaller DOS at the Fermi level (Figure S6). As the distance between atoms decreases, the repulsion of orbitals between $d_{x^2-y^2}$ and degenerate d_{xz} and d_{yz} increases. Unexpectedly, $T_c \approx 17.6$ K at 0 GPa, which is pretty high for TM nitrides. The electronic band structure and Eliashberg spectral function are shown in Figures S7 and S8, respectively. Most importantly, the pressure-induced mutual transformation of the spin state to a superconducting state in $I4/mmm$ is achieved. This is of great significance for the application of spin-to-superconducting switching materials and could be a good pressure gauge.

It is noticed that TM nitrides are widely used as superhard materials due to their outstanding mechanical properties, which are also important for structural stability. The elastic moduli and hardness of MnN_2 are calculated (Tables S2 and S3). They are all mechanically stable. The hardness was calculated using Chen's model (H_{v1})[28] and Zhong's model (H_{v2}).[29] The calculated hardness values from the two methods are almost close. The results show that the AFM-$P2_1/m$-MnN_2 phase is extremely incompressible, with H_v above 20 GPa. This is primarily attributed to two reasons: one is the covalent bonds between nitrogen atoms and the other is the stacking of octahedrons. Although there are strong covalent bonds between the nitrogen atoms, the hardness of $I4/mmm$ in NM and FM states is much less than that of AFM-$P2_1/m$ because the c axis is longer than the a and b axes.

CONCLUSIONS

We find a manganese nitrogen superconductor in $I4/mmm$-MnN_2 by high pressure, which could be a great model for the discussion on the connection between magnetism and superconductivity. It is the first conventional superconductor by pressured-induced magnetic vanishing. The superconducting state can be obtained in two ways: the first is the pressure-induced transition from the AFM $P2_1/m$-MnN_2 phase to nonmagnetic $I4/mmm$ phase at 30 GPa, while the other is the only pressure-induced transition from the ferromagnetic $I4/mmm$ phase to magnetic vanishing at 14 GPa, which pressure could be easily achieved experimentally. In the second way, the edge-sharing tetragonal (MnN_5) pyramids instead of distorted octahedrons (MnN_6) are accompanied by negative compression along the c axis. The $d_{x^2-y^2}$ orbital is pushed above the Fermi level because of increasing crystal-field splitting. Thus, the system transforms from a high-spin state to a low-spin state, driving disappearance of magnetism and emergence of

https://doi.org/10.1021/acsomega.1c03583
ACS Omega 2021, 6, 21830−21836

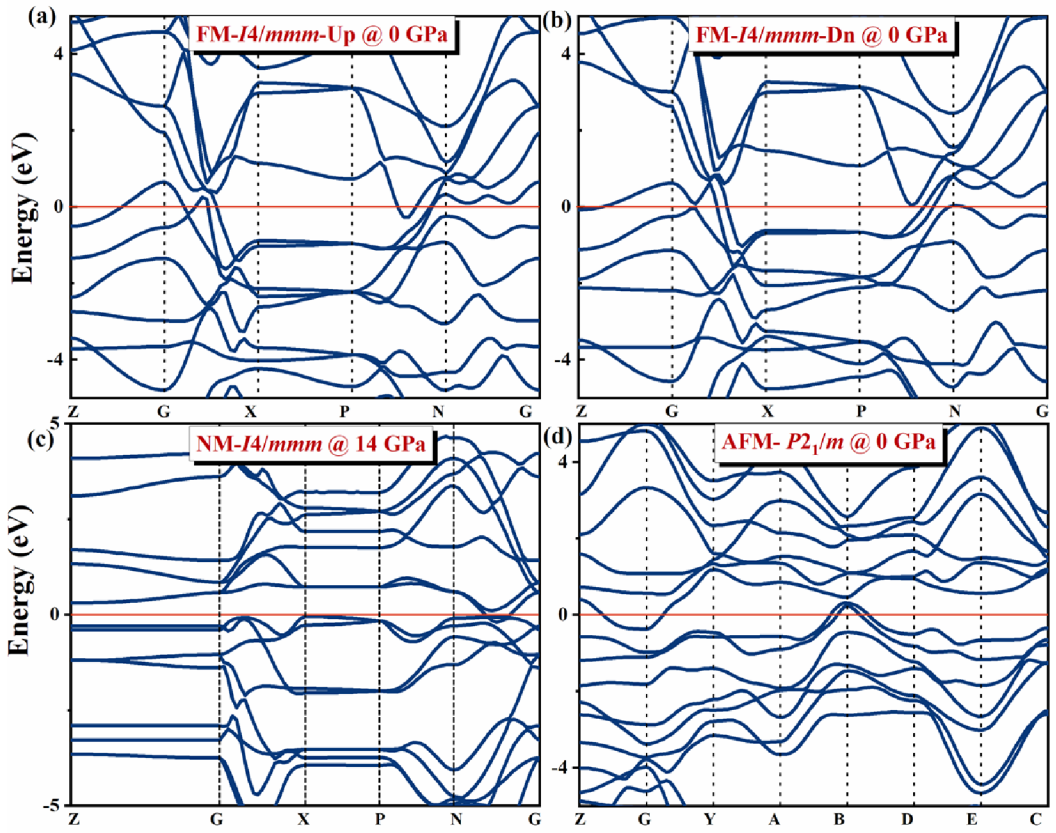

Figure 4. Electronic band structures of MnN_2: (a) and (b) spin up and spin down of the FM-*I*4/*mmm* state at 0 GPa, (c) NM-*I*4/*mmm* state at 14 GPa, and (d) AFM-$P2_1/m$ at 0 GPa.

superconductivity. All of these structures can remain at 0 GPa. We also find that the T_c of the *I*4/*mmm* phase decreases with increasing pressure and can reach 17.6 K at 0 GPa. Remarkably, *I*4/*mmm*-MnN_2 can achieve spin-to-superconducting state mutual transformation by pressure. Moreover, the AFM-$P2_1/m$-MnN_2 phase is extremely incompressible with the hardness value above 20 GPa, which is a potential ultrahard material. This work provides systematic interpretation for the connection between magnetism and superconductivity, which might give good clues to design new spin-to-superconducting switching materials.

COMPUTATIONAL DETAILS

The structure search of Mn−N compounds is performed by the evolutionary algorithm using the variable-composition mode of the USPEX code.[30,31] Structural relaxations, electronic properties, and total energies were calculated using density functional theory (DFT), as implemented in the Vienna ab initio simulation package[32] with the projector augmented wave method.[33] For the exchange−correlation potential, we used the Perdew−Burke−Ernzerhof parameterization of the generalized gradient approximation.[34] A cutoff energy of 850 eV was chosen. Monkhorst−Pack *k*-grid meshes[35] with reciprocal space resolutions of $2\pi \times 0.03$ Å^{-1} and $2\pi \times 0.02$ Å^{-1} were used for thermodynamic calculations and electronic property determination, respectively. For Mn and N, the electronic configurations of $3d^64s^1$ and $2s^22p^3$ were chosen, respectively. Phonon dispersion curves with the PHONOPY code[36] based on a supercell approach with the force constant matrices and EPC were obtained by density functional perturbation theory, as implemented in the Quantum ESPRESSO package.[37] Norm-conserving potentials were used with a kinetic energy cutoff of 90 Ry. The q-point mesh of the electron−phonon interaction matrix element adopted $4 \times 4 \times 4$. Elastic constants are calculated using the strain−stress method, while bulk modulus (B) and shear modulus (G) are derived from the Voigt−Reuss−Hill averaging scheme.[38] We relax lattice parameters and magnetic moment of experimental structures $Pm\bar{3}m$-Mn_4N, *Pbcn*-Mn_2N, *I*4/*mmm*-Mn_3N_2, and *rs*-MnN by GGA and GGA + U (U = 3, 4, 5, and 6 eV) according to other works[39,40] and compare with the experimental results shown in Figure S9. The magnetic moment does not agree well with the experimental results, especially in $Pm\bar{3}m$-Mn_4N. On the contrary, the results of GGA are in good agreement.

ASSOCIATED CONTENT

Supporting Information

The Supporting Information is available free of charge at https://pubs.acs.org/doi/10.1021/acsomega.1c03583.

Thermodynamic stability and phonon spectrum; electronic structure and superconducting properties of *I*4/*mmm*-MnN_2; U value test; and crystal parameters and mechanical properties of MnN_2 (PDF)

AUTHOR INFORMATION

Corresponding Authors

Kuo Bao − *State Key Laboratory of Superhard Materials, College of Physics, Jilin University, Changchun 130012, China;* orcid.org/0000-0002-9330-1384; Email: baokuo@jlu.edu.cn

https://doi.org/10.1021/acsomega.1c03583
ACS Omega 2021, 6, 21830−21836

Tian Cui − *Institute of High Pressure Physics, School of Physical Science and Technology, Ningbo University, Ningbo 315211, China; State Key Laboratory of Superhard Materials, College of Physics, Jilin University, Changchun 130012, China;* orcid.org/0000-0002-9664-848X; Email: cuitian@nbu.edu.cn

Authors

Li Li − *State Key Laboratory of Superhard Materials, College of Physics, Jilin University, Changchun 130012, China*

Xingbin Zhao − *State Key Laboratory of Superhard Materials, College of Physics, Jilin University, Changchun 130012, China*

Defang Duan − *State Key Laboratory of Superhard Materials, College of Physics, Jilin University, Changchun 130012, China;* orcid.org/0000-0002-6878-1830

Complete contact information is available at: https://pubs.acs.org/10.1021/acsomega.1c03583

Notes

The authors declare no competing financial interest.

■ ACKNOWLEDGMENTS

This work was supported by the National Key R&D Program of China (nos. 2018YFA0703404, 2016YFB0201204, and 2017YFA0403704), the National Natural Science Foundation of China (nos. 11774121 and 91745203,), and the Program for Changjiang Scholars and Innovative Research Team in University (no. IRT_15R23). Parts of calculations were performed in the High Performance Computing Center (HPCC) of Jilin University.

■ REFERENCES

(1) Steglich, F.; Aarts, J.; Bredl, C. D.; Lieke, W.; Meschede, D.; Franz, W.; Schäfer, H. Superconductivity in the Presence of Strong Pauli Paramagnetism: $CeCu_2Si_2$. *Phys. Rev. Lett.* **1979**, *43*, 1892−1896.

(2) Kamihara, Y.; Hiramatsu, H.; Hirano, M.; Kawamura, R.; Yanagi, H.; Kamiya, T.; Hosono, H. Iron-Based Layered Superconductor: LaOFeP. *J. Am. Chem. Soc.* **2006**, *128*, 10012−10013.

(3) Wu, W.; Cheng, J.; Matsubayashi, K.; Kong, P.; Lin, F.; Jin, C.; Wang, N.; Uwatoko, Y.; Luo, J. Superconductivity in the Vicinity of Antiferromagnetic Order in CrAs. *Nat. Commun.* **2014**, *5*, No. 5508.

(4) Cheng, J. G.; Matsubayashi, K.; Wu, W.; Sun, J. P.; Lin, F. K.; Luo, J. L.; Uwatoko, Y. Pressure Induced Superconductivity on the Border of Magnetic Order in MnP. *Phys. Rev. Lett.* **2015**, *114*, No. 117001.

(5) Stolyarov, V. S.; et al. Electronic Structures and Surface Reconstructions in Magnetic Superconductor Rbeufe4as4. *J. Phys. Chem. Lett.* **2020**, *11*, 9393−9399.

(6) Dai, P. Antiferromagnetic Order and Spin Dynamics in Iron-Based Superconductors. *Rev. Mod. Phys.* **2015**, *87*, 855−896.

(7) Snider, E.; Dasenbrock-Gammon, N.; McBride, R.; Debessai, M.; Vindana, H.; Vencatasamy, K.; Lawler, K. V.; Salamat, A.; Dias, R. P. Room-Temperature Superconductivity in a Carbonaceous Sulfur Hydride. *Nature* **2020**, *586*, 373−377.

(8) Duan, D.; Liu, Y.; Tian, F.; Li, D.; Huang, X.; Zhao, Z.; Yu, H.; Liu, B.; Tian, W.; Cui, T. Pressure-Induced Metallization of Dense $(H_2S)_2H_2$ with High-T_c Superconductivity. *Sci. Rep.* **2014**, *4*, No. 6968.

(9) Xie, H.; Zhang, W.; Duan, D.; Huang, X.; Huang, Y.; Song, H.; Feng, X.; Yao, Y.; Pickard, C. J.; Cui, T. Superconducting Zirconium Polyhydrides at Moderate Pressures. *J. Phys. Chem. Lett.* **2020**, *11*, 646−651.

(10) Rivadulla, F.; et al. Reduction of the Bulk Modulus at High Pressure in CrN. *Nat. Mater.* **2009**, *8*, 947−951.

(11) Wang, S.; et al. Experimental Invalidation of Phase-Transition-Induced Elastic Softening in CrN. *Phys. Rev. B* **2012**, *86*, No. 064111.

(12) Feng, X.; Bao, K.; Huang, Y.; Ma, S.; Tao, Q.; Zhu, P.; Cui, T. Complete Ligand Reinforcing the Structure of Cubic-CrN. *J. Alloys Compd.* **2019**, *783*, 232−236.

(13) Salke, N. P.; Xia, K.; Fu, S.; Zhang, Y.; Greenberg, E.; Prakapenka, V. B.; Liu, J.; Sun, J.; Lin, J. F. Tungsten Hexanitride with Single-Bonded Armchairlike Hexazine Structure at High Pressure. *Phys. Rev. Lett.* **2021**, *126*, No. 065702.

(14) Baturina, T. I.; Mironov, A. Y.; Vinokur, V. M.; Baklanov, M. R.; Strunk, C. Localized Superconductivity in the Quantum-Critical Region of the Disorder-Driven Superconductor-Insulator Transition in Tin Thin Films. *Phys. Rev. Lett.* **2007**, *99*, No. 257003.

(15) Feng, X.; et al. Role of TM-TM Connection Induced by Opposite d-Electron States on the Hardness of Transition-Metal (TM = Cr, W) Mononitrides. *Inorg. Chem.* **2019**, *58*, 15573−15579.

(16) Binns, J.; Donnelly, M. E.; Pena-Alvarez, M.; Wang, M.; Gregoryanz, E.; Hermann, A.; Dalladay-Simpson, P.; Howie, R. T. Direct Reaction between Copper and Nitrogen at High Pressures and Temperatures. *J. Phys. Chem. Lett.* **2019**, *10*, 1109−1114.

(17) Zhang, W.; Fang, Y.; Zhang, Z.; Tian, F.; Huang, Y.; Wang, X.; Huang, X.; Huang, F.; Cui, T. A New Superconducting 3R-WS_2 Phase at High Pressure. *J. Phys. Chem. Lett.* **2021**, *12*, 3321−3327.

(18) Wen, T.; Wang, Y.; Li, C.; Jiang, D.; Jiang, Z.; Qu, S.; Yang, W.; Wang, Y. Site-Specific Pressure-Driven Spin-Crossover in $Lu_{1-X}Sc_xFeO_3$. *J. Phys. Chem. Lett.* **2020**, *11*, 8549−8553.

(19) Kunes, J.; Lukoyanov, A. V.; Anisimov, V. I.; Scalettar, R. T.; Pickett, W. E. Collapse of Magnetic Moment Drives the Mott Transition in Mno. *Nat. Mater.* **2008**, *7*, 198−202.

(20) Shimizu, K.; Kimura, T.; Furomoto, S.; Takeda, K.; Kontani, K.; Onuki, Y.; Amaya, K. Superconductivity in the Non-Magnetic State of Iron under Pressure. *Nature* **2001**, *412*, 316−318.

(21) Mekata, M. Magnetic Study on Mn_4n and Its Related Compounds. *J. Phys. Soc. Jpn.* **1962**, *17*, 796−803.

(22) Suzuki, K.; Kaneko, T.; Yoshida, H.; Obi, Y.; Fujimori, H.; Morita, H. Crystal Structure and Magnetic Properties of the Compound Mnn. *J. Alloys Compd.* **2000**, *306*, 66−71.

(23) Leineweber, A.; Niewa, R.; Jacobs, H.; Kockelmann, W. The Manganese Nitrides H-Mn_3N_2 and Θ-Mn_6N_5 + X: Nuclear and Magnetic Structures. *J. Mater. Chem.* **2000**, *10*, 2827−2834.

(24) Mekata, M.; Haruna, J.; Takaki, H. Neutron Diffraction Study of Antiferromagnetic Mn_2N. *J. Phys. Soc. Jpn.* **1968**, *25*, 234−238.

(25) Wu, L.; Tian, R.; Wan, B.; Liu, H.; Gong, N.; Chen, P.; Shen, T.; Yao, Y.; Gou, H.; Gao, F. Prediction of Stable Iron Nitrides at Ambient and High Pressures with Progressive Formation of New Polynitrogen Species. *Chem. Mater.* **2018**, *30*, 8476−8485.

(26) Chong, X.; Jiang, Y.; Zhou, R.; Feng, J. Pressure Dependence of Electronic Structure and Superconductivity of the MnX (X = N, P, As, Sb). *Sci. Rep.* **2016**, *6*, No. 21821.

(27) Allen, P. B.; Dynes, R. C. Transition Temperature of Strong-Coupled Superconductors Reanalyzed. *Phys. Rev. B* **1975**, *12*, 905−922.

(28) Chen, X.-Q.; Niu, H.; Li, D.; Li, Y. Modeling Hardness of Polycrystalline Materials and Bulk Metallic Glasses. *Intermetallics* **2011**, *19*, 1275−1281.

(29) Zhong, M.-M.; Kuang, X.-Y.; Wang, Z.-H.; Shao, P.; Ding, L.-P.; Huang, X.-F. Phase Stability, Physical Properties, and Hardness of Transition-Metal Diborides MB_2 (M = Tc, W, Re, and Os): First-Principles Investigations. *J. Phys. Chem. C* **2013**, *117*, 10643−10652.

(30) Lyakhov, A. O.; Oganov, A. R.; Stokes, H. T.; Zhu, Q. New Developments in Evolutionary Structure Prediction Algorithm Uspex. *Comput. Phys. Commun.* **2013**, *184*, 1172−1182.

(31) Oganov, A. R.; Lyakhov, A. O.; Valle, M. How Evolutionary Crystal Structure Prediction Works—and Why. *Acc. Chem. Res.* **2011**, *44*, 227−237.

(32) Kresse, G.; Furthmüller, J. Efficient Iterative Schemes for Ab Initio Total-Energy Calculations Using a Plane-Wave Basis Set. *Phys. Rev. B* **1996**, *54*, No. 11169.

(33) Kresse, G.; Joubert, D. From Ultrasoft Pseudopotentials to the Projector Augmented-Wave Method. *Phys. Rev. B* **1999**, *59*, No. 1758.
(34) Perdew, J. P.; Burke, K.; Ernzerhof, M. Generalized Gradient Approximation Made Simple. *Phys. Rev. Lett.* **1996**, *77*, No. 3865.
(35) Monkhorst, H. J.; Pack, J. D. Special Points for Brillouin-Zone Integrations. *Phys. Rev. B* **1976**, *13*, No. 5188.
(36) Togo, A.; Oba, F.; Tanaka, I. First-Principles Calculations of the Ferroelastic Transition between Rutile-Type Andcacl$_2$-Typesio$_2$at High Pressures. *Phys. Rev. B* **2008**, *78*, No. 134106.
(37) Giannozzi, P.; Baroni, S.; Bonini, N.; Calandra, M.; Car, R.; Cavazzoni, C.; Ceresoli, D.; Chiarotti, G. L.; Cococcioni, M.; Dabo, I. Quantum Espresso: A Modular and Open-Source Software Project for Quantum Simulations of Materials. *J. Phys.: Condens. Matter* **2009**, *21*, No. 395502.
(38) Hill, R. The Elastic Behaviour of a Crystalline Aggregate. *Proc. Phys. Soc. A* **1952**, *65*, 349−354.
(39) Deng, J.; Liu, N.; Guo, J.; Chen, X. Large Spin Gaps in the Half-Metals Mn_4 (M = Mn, Fe, Co) with N_2 Dimers. *Phys. Rev. B* **2019**, *99*, No. 184409.
(40) Wang, S.-S.; Yu, Z.-M.; Liu, Y.; Jiao, Y.; Guan, S.; Sheng, X.-L.; Yang, S. A. Two-Dimensional Nodal-Loop Half-Metal in Monolayer MnN. *Phys. Rev. Mater.* **2019**, *3*, No. 084201.

https://doi.org/10.1021/acsomega.1c03583
ACS Omega 2021, 6, 21830−21836